Electronic Supplementary Material (ESI) for Inorganic Chemistry Frontiers.

Centimeter-sized Novel Two-dimensional Organic Lead-Tin Mixed Iodide Single Crystals for Efficient Photodetector Applications

Xiaomei Jiang,[‡,*a,b] Tiantian Li,[‡,a] Qingzheng Kong,[a] Ying Sun[a] and Xutang Tao[*b]

[a] School of Preventive Medicine Sciences (Institute of Radiation Medicine), Shandong First Medical University & Shandong Academy of Medical Sciences, No. 6699 Qingdao Road, Jinan 250117, People's Republic of China

[b] State Key Laboratory of Crystal Materials, Shandong University, No. 27 Shanda South Road, Jinan 250100, People's Republic of China

[‡]These authors contributed equally.

***Corresponding authors.**

E-mail addresses: jiangxiaomei@sdfmu.edu.cn, txt@sdu.edu.cn

Table S1. Crystal and Refinement Data for $(C_8H_9F_3N)_2Pb_{1-x}Sn_xI_4$(x=0,0.5,1) single crystal

Empirical Formula	$(C_8H_9F_3N)_2PbI_4$	$(C_8H_9F_3N)_2Pb_{0.5}Sn_{0.5}I_4$	$(C_8H_9F_3N)_2SnI_4$
Formula Weight/g·mol^{-1}	1067.11	1022.86	978.61
Crystal System	monoclinic	monoclinic	monoclinic
Space Group	$P2_1/c$(14)	$P2_1/c$(14)	$P2_1/c$(14)
Unit Cell Dimensions	a=18.3980(8)Å b=8.5193(3)Å c=8.7052(3)Å β=97.910(2)°	18.404(4)Å 8.5313(16)Å 8.6674(17)Å β=97.850(4)°	18.3143(10)Å 8.5322(4)Å 8.6166(5)Å β=97.786(2)°
Volume/Å^3	1351.45(9)	1348.1(5)	1334.03
$\rho_{calculated}$/g·mol^{-1}	2.622	2.520	2.436
Z	2	2	2
Index Ranges	-21≤h≤21 -10≤k≤10 -10≤l≤10	-21≤h≤21 -9≤k≤10 -8≤l≤10	-21≤h≤21 -10≤k≤10 -10≤l≤10
Completeness to θ = 25	100%	98.7%	100%
Data/Restraints/Parameters	2382/0/123	2345/142/171	2353/0/123
Goodness-of-Fit	1.062	1.086	1.021
Final R Indices [I > 2σ(I)]	R_{obs}=0.0314 ωR_{obs}=0.0654	R_{obs}=0.0361 ωR_{obs}=0.1078	R_{obs}=0.0644 ωR_{obs}=0.0630
R Indices [all data]	R_{all}=0.0439 ωR_{all}=0.0702	R_{all}=0.0418 ωR_{all}=0.1131	R_{all}=0.0363 ωR_{all}=0.0572
Largest Diff. Peak and Hole	-0.6 and 0.9 e·Å^{-3}	-0.9 and 1.2 e·Å^{-3}	-0.6 and 0.7 e·Å^{-3}
2Theta Range (Data Collection)	2.235 to 24.995	2.234 to 24.995	2.240 to 24.000
CCDC Number	2041929 [Reported]	2234210	2211886

Table S2. Fractional atomic coordinates and equivalent isotropic Displacement Parameters for $(C_8H_9F_3N)_2Pb_{1-x}Sn_xI_4$(x=0,0.5,1).

$(C_8H_9F_3N)_2PbI_4$				
Atom	**x/a**	**y/b**	**z/c**	**U [Å^2]**
Pb1	0.5	0.5	0.5	0.03854(14)
I1	0.32778(3)	0.43545(7)	0.43828(7)	0.05944(19)
I2	0.47029(3)	0.81034(6)	0.29930(6)	0.05504(18)
C1	0.2848(5)	0.9509(12)	0.4259(11)	0.071(3)
C2	0.2209(3)	0.9567(7)	0.5133(6)	0.057(2)
C3	0.2022(3)	0.8229(5)	0.5903(7)	0.065(2)
C4	0.1456(3)	0.8285(5)	0.6809(7)	0.069(3)
C5	0.1078(3)	0.9679(7)	0.6945(7)	0.062(2)
C6	0.1265(3)	1.1018(5)	0.6175(7)	0.071(3)
C7	0.1831(3)	1.0962(6)	0.5269(7)	0.075(3)
C8	0.0516(7)	0.9786(15)	0.7996(16)	0.090(3)
F1	-0.0145(5)	0.9906(13)	0.7237(12)	0.175(4)
F2	0.0439(5)	0.8528(12)	0.8795(11)	0.167(4)
F3	0.0574(6)	1.0905(13)	0.8892(13)	0.221(7)
N1	0.3503(4)	1.0236(8)	0.5193(9)	0.067(2)
H1A	0.3908	0.9912	0.4836	0.081
H1B	0.3521	0.9954	0.6182	0.081
H1C	0.3472	1.1277	0.5118	0.081
H1D	0.2731	1.0068	0.3286	0.085
H1E	0.2954	0.8426	0.4026	0.085
H3	0.2275	0.7296	0.5812	0.078
H4	0.1331	0.7389	0.7324	0.083
H6	0.1012	1.1951	0.6266	0.085
H7	0.1956	1.1857	0.4754	0.09
$(C_8H_9F_3N)_2Pb_{0.5}Sn_{0.5}I_4$				
Atom	**x/a**	**y/b**	**z/c**	**U [Å^2]**
Pb1	0	0.5	0	0.03453(18)
Sn1	0	0.5	0	0.03453(18)
I1	0.17133(3)	0.43646(6)	0.06123(6)	0.0535(2)
I2	0.02869(3)	0.80555(5)	0.20441(5)	0.0491(2)
C1	0.2149(5)	0.5481(12)	0.5771(11)	0.066(2)
C2	0.2780(4)	0.5416(10)	0.4892(10)	0.0516(17)
C3	0.2979(5)	0.6772(11)	0.4117(11)	0.064(2)
C3B	0.4415(13)	0.519(4)	0.199(2)	0.081(5)
C4	0.3563(6)	0.6698(11)	0.3197(11)	0.068(2)
C5	0.3918(5)	0.5317(10)	0.3011(11)	0.0593(17)
C6	0.3720(5)	0.3990(11)	0.3823(12)	0.066(2)
C7	0.3168(5)	0.4050(10)	0.4734(11)	0.062(2)

C8	0.4490(7)	0.5260(16)	0.2081(15)	0.091(2)
F1	0.5170(5)	0.5189(16)	0.2861(15)	0.109(3)
F1B	0.5034(15)	0.438(4)	0.237(4)	0.089(7)
F2	0.4586(6)	0.6562(13)	0.1270(13)	0.109(3)
F2B	0.4204(17)	0.585(4)	0.062(3)	0.090(6)
F3	0.4162(14)	0.463(4)	0.055(3)	0.085(6)
F3B	0.4500(7)	0.3961(13)	0.1202(15)	0.114(3)
N1	0.1477(4)	0.4747(8)	0.4858(9)	0.0605(18)
H1A	0.15	0.4842	0.3843	0.073
H1B	0.1077	0.5229	0.5089	0.073
H1C	0.1458	0.3736	0.5103	0.073
H1D	0.2045	0.6565	0.5999	0.079
H1E	0.2269	0.4932	0.6752	0.079
H3	0.273	0.771	0.4206	0.076
H4	0.3704	0.7601	0.2716	0.082
H6	0.3969	0.3052	0.3739	0.079
H7	0.3051	0.3152	0.5258	0.075
		$(C_8H_9F_3N)_2SnI_4$		
Atom	**x/a**	**y/b**	**z/c**	**U [Å^2]**
Sn1	0.5	1	0.5	0.0373(2)
I1	0.52773(3)	0.80061(5)	0.20851(6)	0.05400(18)
I2	0.32929(3)	0.93706(6)	0.43917(6)	0.05812(19)
C1	0.2865(5)	0.4514(10)	0.4174(10)	0.069(2)
C2	0.2219(2)	0.4578(6)	0.5084(6)	0.055(2)
C3	0.2030(3)	0.3238(5)	0.5856(6)	0.059(2)
C4	0.1464(3)	0.3294(5)	0.6780(6)	0.067(2)
C5	0.1089(3)	0.4689(7)	0.6933(6)	0.063(2)
C6	0.1278(3)	0.6029(5)	0.6162(7)	0.076(3)
C7	0.1844(3)	0.5973(5)	0.5237(6)	0.071(3)
C8	0.0523(6)	0.4800(14)	0.7980(15)	0.091(3)
F1	-0.0130(4)	0.4953(12)	0.7251(10)	0.181(4)
F2	0.0596(5)	0.5883(12)	0.8938(12)	0.237(7)
F3	0.0441(5)	0.3549(10)	0.8773(9)	0.164(3)
N1	0.3529(3)	0.5230(7)	0.5119(8)	0.069(2)
H1A	0.3933	0.4938	0.4725	0.082
H1B	0.3558	0.4907	0.6108	0.082
H1C	0.349	0.6269	0.5085	0.082
H1D	0.2969	0.3433	0.3931	0.083
H1E	0.2748	0.5079	0.3195	0.083
H3	0.2281	0.2305	0.5753	0.071
H4	0.1337	0.2397	0.7297	0.08
H6	0.1027	0.6962	0.6264	0.091

H7	0.1971	0.687	0.4721	0.085

Table S3. Bond lengths of $(C_8H_9F_3N)_2Pb_{1-x}Sn_xI_4$(x=0,0.5,1).

$(C_8H_9F_3N)_2PbI_4$		**$(C_8H_9F_3N)_2SnI_4$**	
Atoms	**d**	**Atoms**	**d**
Pb1—I2	3.1747(5)	Sn1—I1^{i}	3.1315(5)
Pb1—I2^{i}	3.1765(5)	Sn1—I1^{ii}	3.1332(5)
Pb1—I2^{ii}	3.1747(5)	Sn1—I1	3.1315(5)
Pb1—I2^{iii}	3.1765(5)	Sn1—I1^{iii}	3.1332(5)
Pb1—I1^{ii}	3.1878(6)	Sn1—I2	3.1454(6)
Pb1—I1	3.1878(6)	Sn1—I2^{i}	3.1454(6)
I2—Pb1^{iv}	3.1765(5)	I1—Sn1^{iv}	3.1332(5)
N1—C1	1.4924(114)	N1—C1	1.4989(101)
C1—C2	1.4865(115)	F3—C8	1.2871(149)
F3—C8	1.2271(173)	C2—C7	1.3893(67)
F1—C8	1.3057(152)	C2—C3	1.3899(70)
F2—C8	1.2960(167)	C2—C1	1.5063(105)
C6—C5	1.3901(79)	C7—C6	1.3914(83)
C6—C7	1.3909(87)	C6—C5	1.3895(77)
C5—C4	1.3902(75)	C5—C4	1.3893(75)
C5—C8	1.4747(155)	C5—C8	1.4665(139)
C4—C3	1.3909(87)	C4—C3	1.3908(81)
C3—C2	1.3894(77)	F1—C8	1.2800(129)
C2—C7	1.3902(79)	F2—C8	1.2342(160)
$(C_8H_9F_3N)_2Pb_{0.5}Sn_{0.5}I_4$			
Atoms	**d**	**Atoms**	**d**
Pb1|Sn1—I2^{i}	3.1555(6)	C4—C3	1.425(15)
Pb1|Sn1—I2^{ii}	3.1566(6)	C5—C6	1.406(12)
Pb1|Sn1—I2	3.1556(6)	C5—C3B	1.359(15)
Pb1|Sn1—I2^{iii}	3.1566(6)	C5—C8	1.411(12)
Pb1|Sn1—I1	3.1719(8)	C7—C6	1.371(13)
Pb1|Sn1—I3^{i}	3.1720(8)	Pb01|Sn01—I002^{ii}	3.1566(6)
I2—Pb1|Sn1^{iv}	3.1566(6)	Pb01|Sn01—I002^{i}	3.1555(6)
I2—Pb1|Sn1^{iv}	3.1566(6)	Pb01|Sn01—I002^{iii}	3.1566(6)
I2—Pb1|Sn1	3.1556(6)	Pb01|Sn01—I003^{i}	3.1720(8)
I1—Pb1|Sn1	3.1719(8)	F1B—C3B	1.329(15)
N1—C1	1.509(11)	F2B—C3B	1.333(15)
C2—C7	1.383(12)	C3B—F4B	1.363(16)
C2—C3	1.412(13)	C3A—F4A	1.346(12)
C2—C1	1.474(12)	C3A—F2A	1.340(12)
C4—C5	1.368(14)	C3A—F1A	1.339(12)
(i) -x, 1-y, -z; (ii) x, 1.5-y, -0.5+z; (iii) -x, -0.5+y, 0.5-z; (iv) -x, 0.5+y, 0.5-z.			

Table S4. Bond angles of $(C_8H_9F_3N)_2Pb_{1-x}Sn_xI_4$(x=0,0.5,1).

$(C_8H_9F_3N)_2PbI_4$		**$(C_8H_9F_3N)_2SnI_4$**	
Atoms	**Angle**	**Atoms**	**Angle**
I2—Pb1—I2^{ii}	180.000	I1^{i}—Sn1—I1	180.000
I2^{ii}—Pb1—I2^{i}	89.528(13)	I1—Sn1—I1^{ii}	90.923(12)
I2—Pb1—I2^{i}	90.472(13)	I1^{i}—Sn1—I1^{ii}	89.077(12)
I2—Pb1—I2^{iii}	89.528(13)	I1^{i}—Sn1—I1^{iii}	90.923(12)
I2^{ii}—Pb1—I2^{iii}	90.472(13)	I1—Sn1—I1^{iii}	89.077(12)
I2^{iii}—Pb1—I2^{i}	180.000	I1^{iii}—Sn1—I1^{ii}	180.000(12)
I2^{iii}—Pb1—I1	86.948(15)	I1^{ii}—Sn1—I2	87.937(14)
I2—Pb1—I1	87.653(15)	I1—Sn1—I2	92.242(14)
I2^{i}—Pb1—I1^{ii}	86.948(15)	I1^{i}—Sn1—I2	87.758(14)
I2^{ii}—Pb1—I1^{ii}	87.653(15)	I1^{iii}—Sn1—I2^{i}	87.937(14)
I2^{ii}—Pb1—I1	92.347(15)	I1^{iii}—Sn1—I2	92.063(14)
I2^{iii}—Pb1—I1^{ii}	93.052(15)	I1^{ii}—Sn1—I2^{i}	92.063(14)
I2—Pb1—I1^{ii}	92.347(15)	I1^{i}—Sn1—I2^{i}	92.242(14)
I2^{i}—Pb1—I1	93.052(15)	I1—Sn1—I2^{i}	87.758(14)
I1^{ii}—Pb1—I1	180.000	I2^{i}—Sn1—I2	180.000
Pb1—I2—Pb1^{iv}	147.035(18)	Sn1—I1—Sn1^{iv}	150.849(16)
C2—C1—N1	110.094(689)	C7—C2—C3	120.062(443)
C5—C6—C7	119.970(503)	C7—C2—C1	120.909(491)
C6—C5—C8	119.314(691)	C3—C2—C1	118.908(494)
C4—C5—C6	120.035(496)	C6—C7—C2	120.000(445)
C4—C5—C8	120.486(681)	C7—C6—C5	119.922(482)
C3—C4—C5	119.961(482)	C6—C5—C8	118.921(642)
C4—C3—C2	120.022(489)	C4—C5—C6	120.079(493)
C3—C2—C1	119.041(578)	C4—C5—C8	120.889(635)
C7—C2—C1	120.807(586)	C3—C4—C5	120.007(470)
C7—C2—C3	120.017(506)	C4—C3—C2	119.932(447)
C2—C7—C6	119.995(496)	N1—C1—C2	109.821(631)
F3—C8—F1	104.732(1186)	F3—C8—C5	114.586(947)
F3—C8—F2	107.920(1162)	F1—C8—F3	100.175(1009)
F3—C8—C5	115.805(1125)	F1—C8—C5	113.327(878)
F1—C8—C5	112.001(1009)	F2—C8—F3	106.003(1055)
F2—C8—F1	99.982(1095)	F2—C8—C5	115.992(1018)
F2—C8—C5	114.809(1047)	F2—C8—F1	105.143(1061)

(i) 1-x, 2-y, 1-z; (ii) 1-x, 0.5+y, 0.5-z; (iii) x, 1.5-y, 0.5+z; (iv) 1-x, -0.5+y, 0.5-z.

$(C_8H_9F_3N)_2Pb_{0.5}Sn_{0.5}I_4$			
Atoms	**Angle**	**Atoms**	**Angle**
I2^{i}—Pb1|Sn1—I2	180.000	C4—C5—C6	118.2(8)
I2—Pb1|Sn1—I2^{iii}	90.696(14)	C4—C5—C8	120.2(9)

I2^{i}—Pb1|Sn1—I2^{iii}	89.304(15)	C6—C5—C8	121.5(9)
I2^{i}—Pb1|Sn1—I2^{ii}	90.696(15)	C3B—C5—C4	121.4(16)
I2—Pb1|Sn1—I2^{ii}	89.304(14)	C3B—C5—C6	120.3(17)
I2^{ii}—Pb1|Sn1—I2^{iii}	180.000(19)	C6—C7—C2	121.4(8)
I2^{ii}—Pb1|Sn1—I1^{i}	92.696(15)	C2—C3—C4	119.6(9)
I2^{i}—Pb1|Sn1—I1^{i}	87.761(14)	C7—C6—C5	121.4(8)
I2^{iii}—Pb1|Sn1—I1	92.696(15)	C5—C3B—F3	117(2)
I2—Pb1|Sn1—I1	87.760(14)	F2B—C3B—C5	114.1(18)
I2—Pb1|Sn1—I1^{i}	92.240(14)	F2B—C3B—F1B	125.(2)
I2^{ii}—Pb1|Sn1—I1	87.304(15)	F2B—C3B—F3	45.(2)
I2^{i}—Pb1|Sn1—I1	92.238(14)	F1B—C3B—C5	120.9(19)
I2^{iii}—Pb1|Sn1—I1^{i}	87.304(15)	F1B—C3B—F3	102(3)
I1—Pb1|Sn1—I1^{i}	180.000	F3B—C8—C5	114.9(10)
Pb1|Sn1—I2—Pb1|Sn1^{iv}	148.884(18)	F1—C8—C5	115.5(11)
C2—C1—N1	111.1(7)	F1—C8—F3B	99.4(11)
C7—C2—C3	118.2(8)	F2—C8—C5	115.7(11)
C7—C2—C1	122.5(8)	F2—C8—F3B	111.9(12)
C3—C2—C1	119.3(9)	F2—C8—F1	96.9(11)
C5—C4—C3	120.9(9)		
(i) 1-x, 2-y, 1-z; (ii) 1-x, 0.5+y, 0.5-z; (iii) x, 1.5-y, 0.5+z; (iv) 1-x, -0.5+y, 0.5-z.			

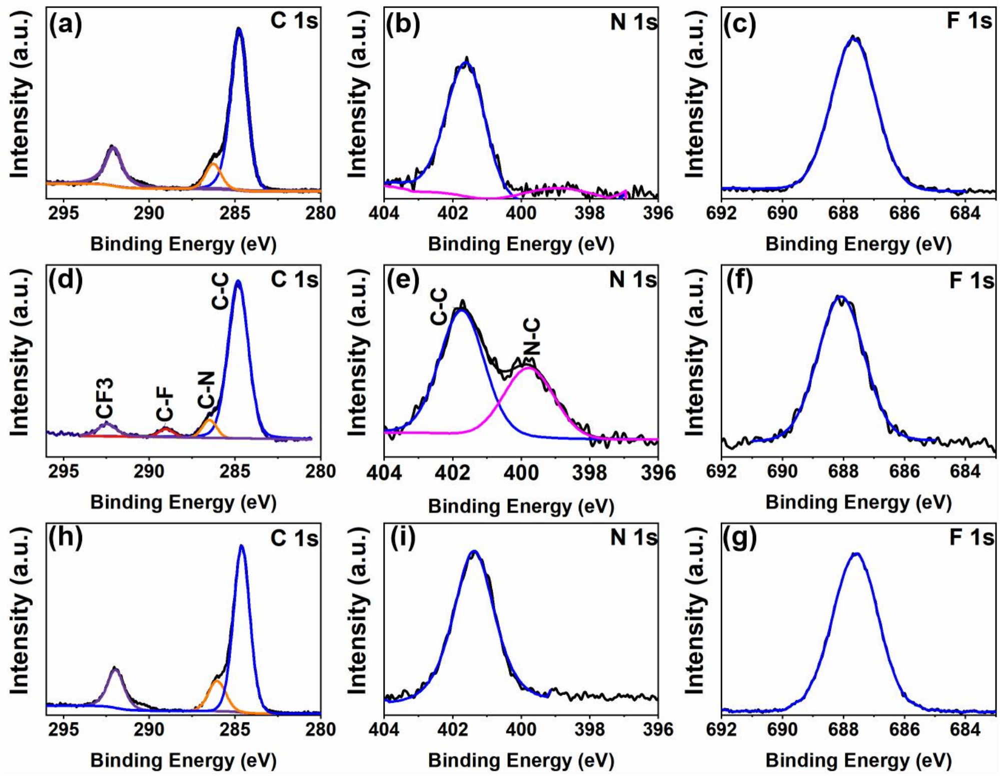

Fig. S1. High-resolution XPS spectra of $(C_8H_9F_3N)_2Pb_{1-x}Sn_xI_4$(x=0,0.5,1) single crystal. (a)-(c) $(C_8H_9F_3N)_2PbI_4$, (d-f) $(C_8H_9F_3N)_2Pb_{0.5}Sn_{0.5}I_4$, and (h-g) $(C_8H_9F_3N)_2SnI_4$.

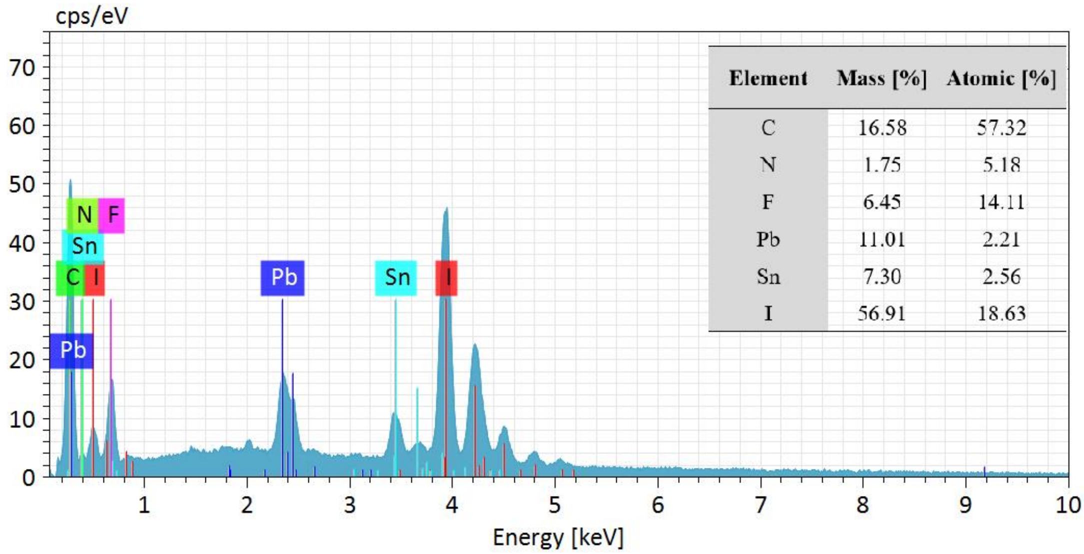

Fig. S2. SEM-EDS results of $(C_8H_9F_3N)_2Pb_{0.5}Sn_{0.5}I_4$ single crystal.

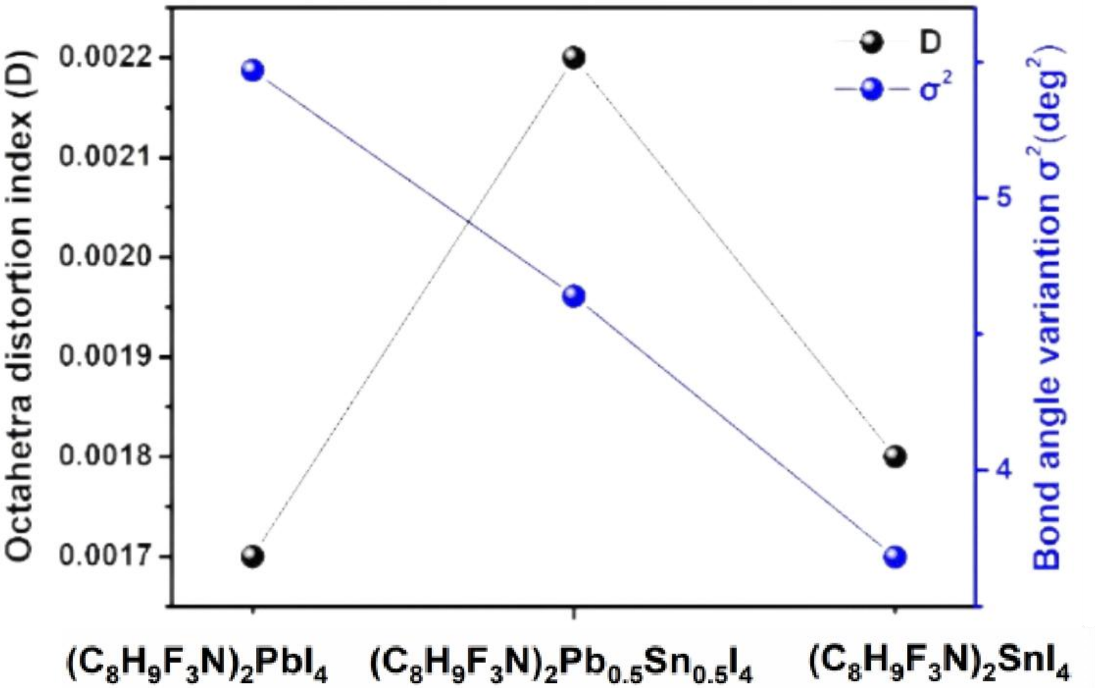

Fig. S3. Distortion Index (D), Bond Angle Variance (σ^2), and bandgap of $(C_8H_9F_3N)_2Pb_{1-x}Sn_xI_4$(x=0,0.5,1).

Table S5. Distortion index (D), bond angle variance (σ^2), and bandgap of $(C_8H_9F_3N)_2Pb_{1-x}Sn_xI_4$(x=0,0.5,1).

	$(C_8H_9F_3N)_2PbI_4$	$(C_8H_9F_3N)_2Pb_{0.5}Sn_{0.5}I_4$	$(C_8H_9F_3N)_2SnI_4$
Equatorial I-M-I angle (deg)	89.528	90.696	90.923
	90.472	89.304	89.077
	86.948	87.761	87.937
Axial I-M-I angle (deg)	87.653	87.305	92.242
	92.347	92.239	87.758
	93.052	92.695	92.063
M-I-M angle (deg)	147.035	150.849	148.884
D	0.0017	0.0022	0.0018
σ^2	5.47	4.64	3.68
Band gap (eV)	2.39	1.96	2.0

Table S6. Water contact angle of $(C_8H_9F_3N)_2Pb_{1-x}Sn_xI_4$(x=0,0.5,1).

Perovskite	**Water contact angle（deg）**
$Cs_2AgBiBr_6/SnO_2/ZnO$[1]	15
$Cs_2AgBiBr_6/ZnO$[1]	48
3D $MAPbI_3$[2]	38.88
$FAPbI_3$[3]	46.9
$(iBA)_2PbI_4$[4]	46.2
$iBA(DMPDA)_{0.5}PbI_4$[4]	50.7
$Cs_2AgBiBr_6$[5]	50.2
$(FAPbI_3)_{0.95}(MAPbBr_3)_{0.05}$[6]	54.6
$(C_8H_9F_3N)_2PbI_4$ (This work)	58.25
$(C_8H_9F_3N)_2Pb_{0.5}Sn_{0.5}I_4$ (This work)	60.25
$(C_8H_9F_3N)_2SnI_4$ (This work)	50.00

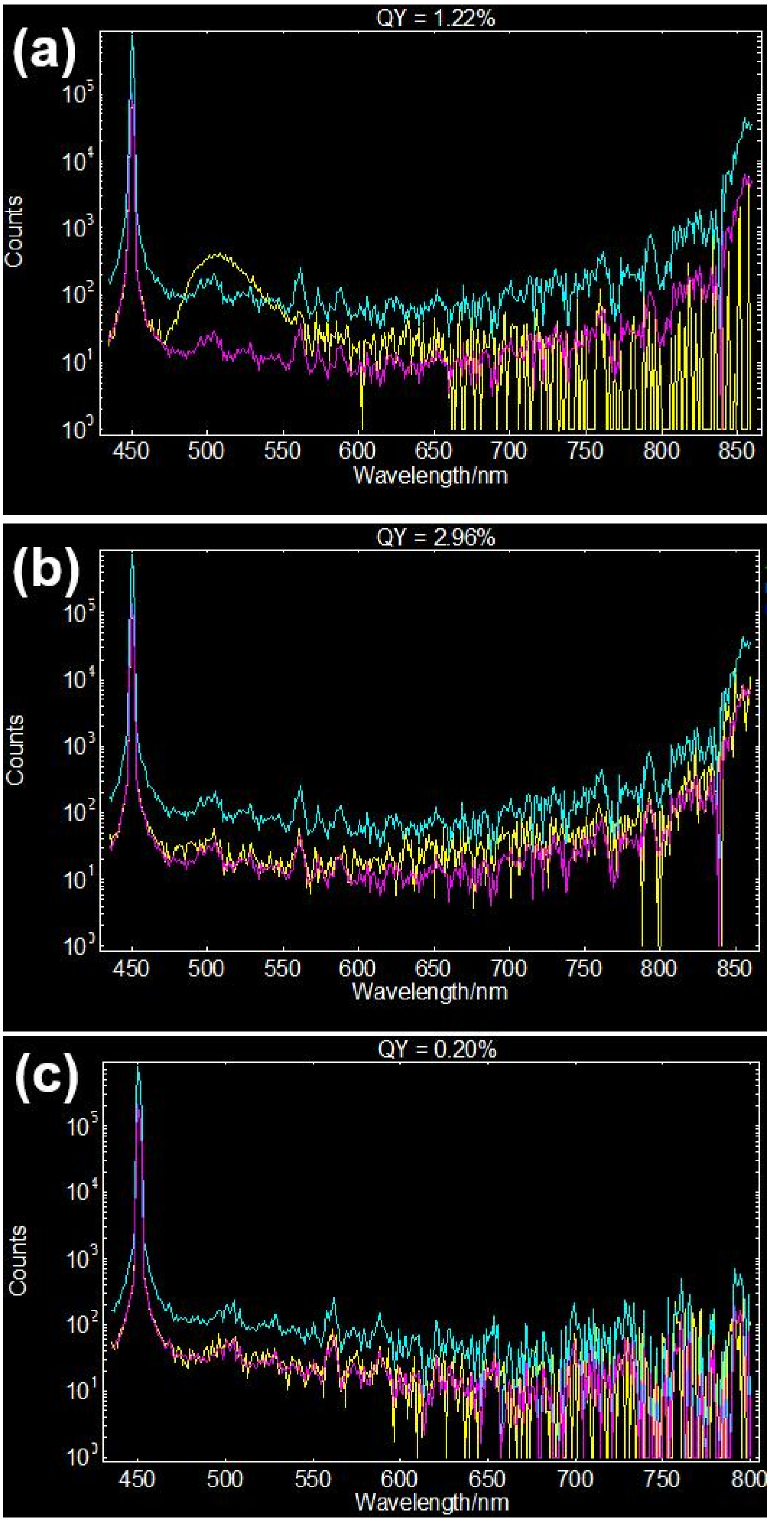

Fig. S4. PLQY results of $(C_8H_9F_3N)_2Pb_{1-x}Sn_xI_4$(x=0,0.5,1). (a) $(C_8H_9F_3N)_2PbI_4$, (b) $(C_8H_9F_3N)_2Pb_{0.5}Sn_{0.5}I_4$, and (c) $(C_8H_9F_3N)_2SnI_4$.

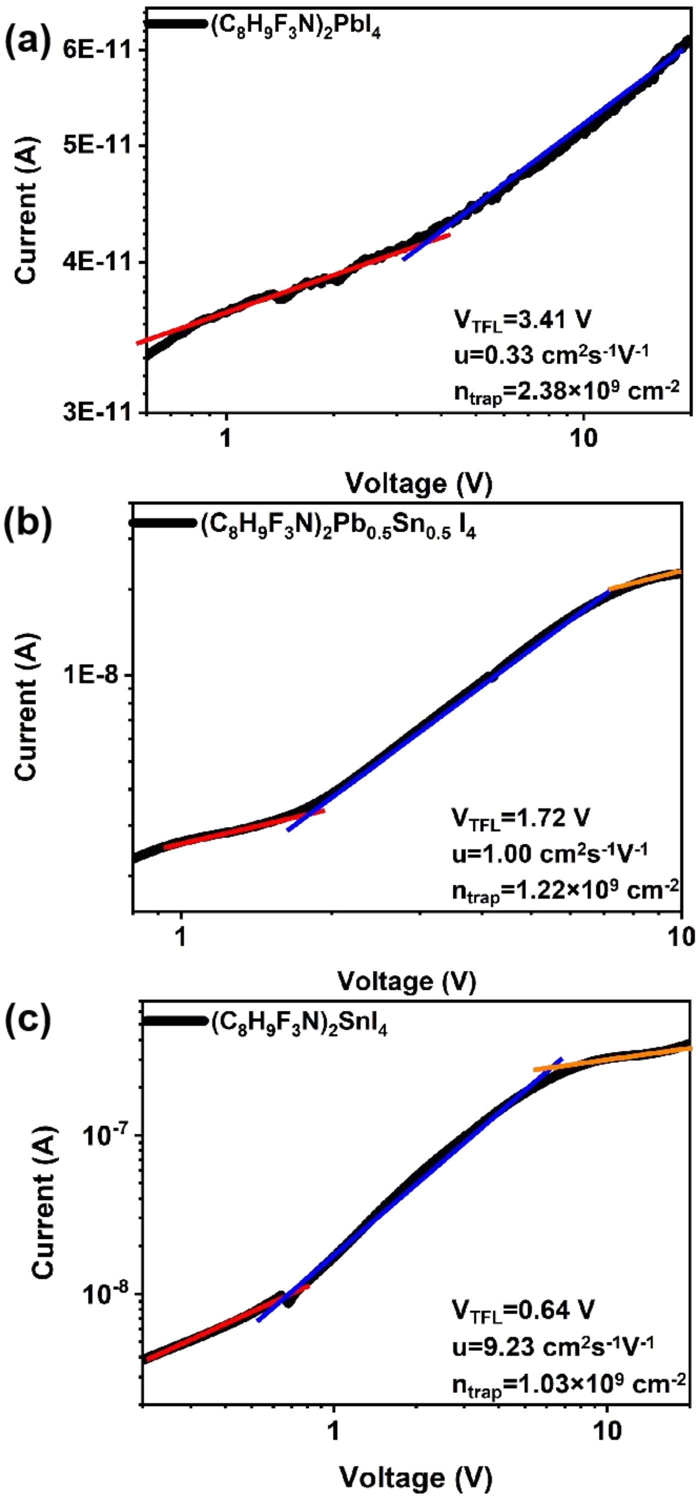

Fig. S5. Current-voltage curves and trap density at 298 K. Characteristic *I-V* curves with two different regimes for (a) $(C_8H_9F_3N)_2PbI_4$ and three different regimes for (b) $(C_8H_9F_3N)_2Pb_{0.5}Sn_{0.5}I_4$ and (c) $(C_8H_9F_3N)_2SnI_4$. A linear Ohmic regime ($I \propto V$, red line) is followed by the trap-filled regime (TFL), marked by a steep increase in current ($I \propto V^n$ (n>3)). The orange line denotes the trap-free Child's regime($I \propto V^2$).

Table S7. The performances of Sn-containing perovskite-based photodetectors.

Materials	**Light intensity ($\mu W\ cm^{-2}$)**	**On/off current ratio**	**R ($A\ W^{-1}$)**	**D* (Jones)**
PEA_2SnI_4 film (30% SnF_2)[7]	2000	/	207.5	2.53×10^{13}
$FASnI_3$ Film[8]	0.064	/	10^5	1.9×10^{12}
$TBASnCl_3$ QDs[9]	360	67	0.0148	5.04×10^{10}
$TBASnCl_3$ (0.03 M SnF_2) QDs[9]	360	238	0.0097	7.67×10^{10}
$MAPb_{0.5}Sn_{0.5}I_3$ thin films[10]	614.3	/	0.0016	3.08×10^{10}
$(PEA)_2SnI_4/MoS_2$[11]	36 pw	10^2	0.121	8.09×10^9
(rGO/PEDOT:PSS)/$(PEA)_2SnI_4$[12]	56.9	/	16	1.92×10^{11}
$TiO_2/CsSnI_3$/P3HT[13]	/	/	0.257	1.5×10^{11}
$CsSnI_3$[14]	/	1.08	0.054	3.85×10^5
$CH_3NH_3Pb_{0.7}Sn_{0.3}I_3$[15]	/	/	0.39	7×10^{12}
$(PEA)_2SnI_4$ microsheets[16]	195.8	10	3.29×10^3	2.06×10^{11}
$(C_8H_9F_3N)_2PbI_4$ (This work)	7000	10^3	0.0138	8.7×10^{10}
$(C_8H_9F_3N)_2Pb_{0.5}Sn_{0.5}I_4$ (This work)	7000	48	0.6681	8.6×10^{10}
$(C_8H_9F_3N)_2SnI_4$ (This work)	7000	18	0.0323	4.7×10^9

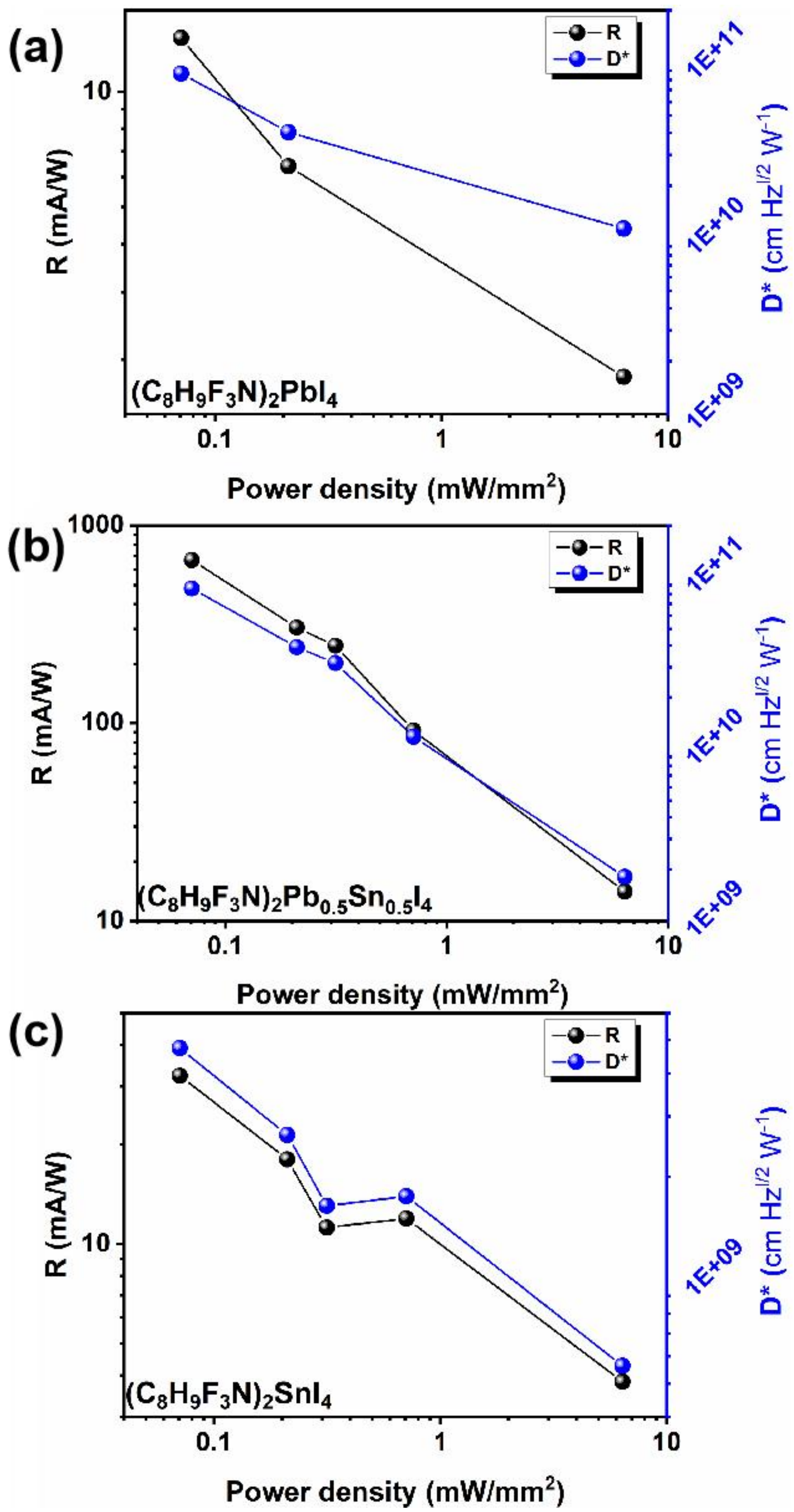

Fig. S6. Relationship of responsivity (R) and detectivity (D^*) with light power density at 10 V. (a) $(C_8H_9F_3N)_2PbI_4$, (b) $(C_8H_9F_3N)_2Pb_{0.5}Sn_{0.5}I_4$, and (c) $(C_8H_9F_3N)_2SnI_4$.

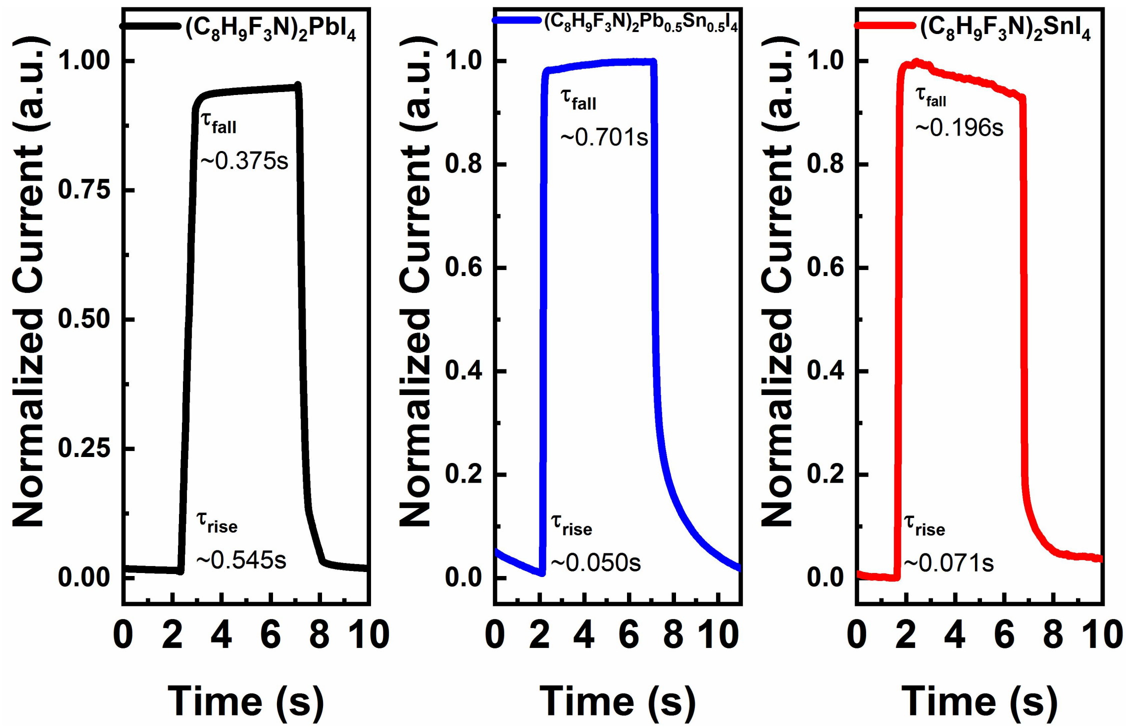

Fig. S7. Temporal response of $(C_8H_9F_3N)_2Pb_{1-x}Sn_xI_4$(x=0,0.5,1) single crystal-based photodetectors at the light intensity of 20 mWcm^{-2} under a bias of 5V. (a) $(C_8H_9F_3N)_2PbI_4$, (b) $(C_8H_9F_3N)_2Pb_{0.5}Sn_{0.5}I_4$, and (c) $(C_8H_9F_3N)_2SnI_4$.

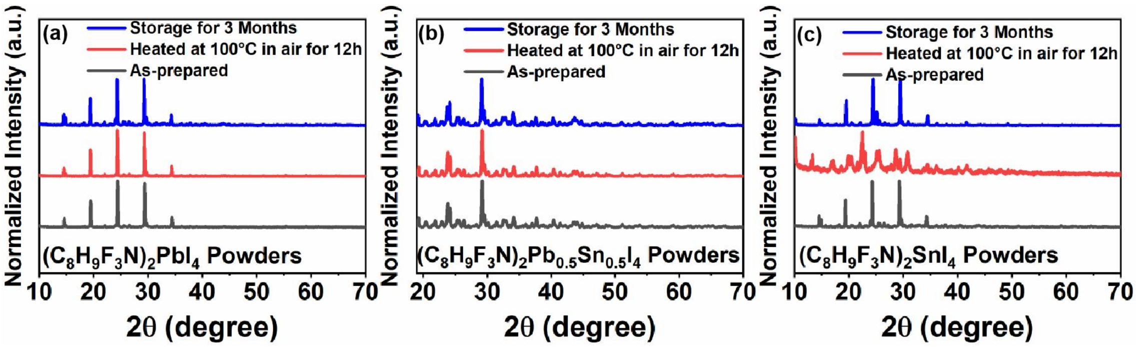

Fig. S8. Stability test. (a)-(c) PXRD patterns of $(C_8H_9F_3N)_2Pb_{1-x}Sn_xI_4$(x=0,0.5,1) powders that storaged in ambient environment (T=24-30°C, RH=45-65%) for above 3 months.

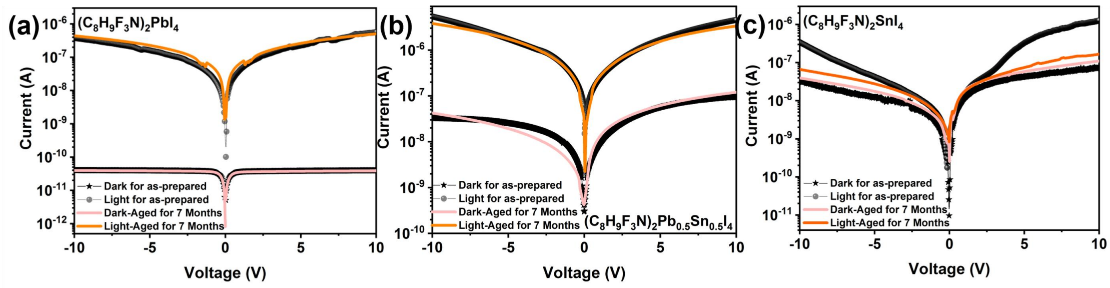

Fig. S9. Stability test. I-V curves for (a) $(C_8H_9F_3N)_2PbI_4$, (b) $(C_8H_9F_3N)_2Pb_{0.5}Sn_{0.5}I_4$, and (c) $(C_8H_9F_3N)_2SnI_4$ with the device architecture of Au/BCP/C_{60}/$(C_8H_9F_3N)_2Pb_{1-x}Sn_xI_4$ (x=0,0.5,1) single crystal/C_{60}/BCP/Au under the illumination of 405 nm laser (P=6.37 mW/mm^2).

References

[1] W. Shen, U. Jung, Z. Xian, B. Jung and J. Park, Enhanced device performance of $Cs_2AgBiBr_6$ double perovskite photodetector by SnO_2/ZnO double electron transport layer, *J. Alloys Compd.*, 2022, **929**, 167329.

[2] N. Guo, Z. Zhou, J. Ni, H.-K. Cai, J.-J. Zhang, Y.-Y. Sun and J. Li, Thin film transistor based on two-dimensional organic-inorganic hybrid perovskite, *Acta Phys. Sin.*, 2020, **69**198102.

[3] R. Yu, G. Wu, R. Shi, Z. Ma, Q. Dang, Y. Qing, C. Zhang, K. Xu and Z. a. Tan, Multidentate coordination induced crystal growth regulation and trap passivation enables over 24% efficiency in perovskite solar cells, *Adv. Energy Mater.*, 2022, **13,** 2203127.

[4] Z. Lai, F. Wang, Y. Meng, X. Bu, X. Kang, Q. Quan, W. Wang, C. Liu, S. Yip and J. C. Ho, Superior performance and stability of 2D dion-jacobson halide perovskite photodetectors operated under harsh conditions without encapsulation, *Adv. Opt. Mater.*, 2021, **9**, 2101523.

[5] R. Li, H. Jiang, Y. Yao, H. Ye, X. Liu, S. Chen and J. Luo, Bulk single crystals of a narrow band gap three-dimensional hybrid perovskitoid enabling ultrastable photodetection, *Chem. Mater.*, 2022, **34**, 10382-10389.

[6] X. Wu, L. Zhang, Z. Xu, S. Olthof, X. Ren, Y. Liu, D. Yang, F. Gao and S. Liu, Efficient perovskite solar cells via surface passivation by a multifunctional small organic ionic compound, *J. Mater. Chem. A*, 2020, **8**, 8313-8322.

[7] K. R. Yun, T. J. Lee, S. K. Kim, J. H. Kim and T. Y. Seong, Fast and highly sensitive photodetectors based on Pb-free Sn-based perovskite with additive engineering, *Adv. Opt. Mater.*, 2022, **11**, 2201974.

[8] C. K. Liu, Q. Tai, N. Wang, G. Tang, H. L. Loi and F. Yan, Sn-based perovskite for highly sensitive photodetectors, *Adv. Sci.*, 2019, **6**, 1900751.

[9] Z. Zhang, S. Yang, J. Hu, H. Peng, H. Li, P. Tang, Y. Jiang, L. Tang and B. Zou, One-pot synthesis of novel ligand-free tin(II)-based hybrid metal halide perovskite quantum dots with high anti-water stability for solution-processed UVC photodetectors, *Nanoscale*, 2022, **14**, 4170-4180.
[10] J. Wu, Y. Zhang, S. Yang, Z. Chen and W. Zhu, Thin $MAPb_{0.5}Sn_{0.5}I_3$ Perovskite single vrystals for sensitive infrared light detection, *Front. Chem.*, 2021, **9**, 821699.
[11] C. Fang, H. Wang, Z. Shen, H. Shen, S. Wang, J. Ma, J. Wang, H. Luo and D. Li, High-performance photodetectors based on lead-free 2D ruddlesden-popper perovskite/MoS_2 heterostructures, *ACS Appl. Mater. Interfaces*, 2019, **11**, 8419-8427.
[12] L. Qian, Y. Sun, M. Wu, C. Li, D. Xie, L. Ding and G. Shi, A lead-free two-dimensional perovskite for a high-performance flexible photoconductor and a light-stimulated synaptic device, *Nanoscale*, 2018, **10**, 6837-6843.
[13] F. Cao, W. Tian, M. Wang, M. Wang and L. Li, Stability enhancement of lead-free $CsSnI_3$ perovskite photodetector with reductive ascorbic acid additive, *InfoMat*, 2020, **2**, 577-584.
[14] M. Han, J. Sun, M. Peng, N. Han, Z. Chen, D. Liu, Y. Guo, S. Zhao, C. Shan, T. Xu, X. Hao, W. Hu and Z.-x. Yang, Controllable Growth of Lead-Free All-inorganic perovskite nanowire array with fast and stable near-infrared photodetection, *J. Phys. Chem. C*, 2019, **123**, 17566-17573.
[15] Y. Wang, D. Yang, D. Ma, D. H. Kim, T. Ahamad, S. M. Alshehri and A. Vadim, Organic-inorganic hybrid Sn-based perovskite photodetectors with high external quantum efficiencies and wide spectral responses from 300 to 1000 nm, *Science China Materials*, 2018, **62**, 790-796.
[16] L. Qian, Y. Sun, M. Sun, Z. Fang, L. Li, D. Xie, C. Li and L. Ding, 2D perovskite microsheets for high-performance photodetectors, *J. Mater. Chem C*, 2019, **7**, 5353-5358.